Effective sea ice area based on a thickness threshold

Victoria L. Ford[1] · Oliver W. Frauenfeld[1] · Christopher J. Nowotarski[2] · Rodrigo J. Bombardi[1]

Abstract

As Arctic sea ice declines in response to climate change, a shift from thick multiyear ice to a thinner ice cover is occurring. With this transition, ice thicknesses approach a threshold below which ice no longer insulates the atmosphere from oceanic surface fluxes. While this is well known, there are no estimates of the magnitude of this threshold, nor of the proportion of sea ice area that is below this threshold as ice thins. We determine this threshold by simulating the atmospheric response to varying thicknesses, ranging from 0.0 to 2.0 m and determine that threshold to be 0.40–0.50 m. The resulting "effective" ice area is 4–14% lower than reported total ice area, as $0.39–0.97 \times 10^6$ km^2 of the total ice area falls below the threshold throughout the twentieth century, including during notable ice minima. The atmosphere above large non-insulating ice-covered regions is susceptible to more than 2 °C of warming despite ice presence. Observed mean Arctic Ocean ice thickness is projected to fall below this threshold as early as the mid-2020s. Studies on ocean–atmosphere interactions in relation to sea ice area should focus on this insulating sea ice area, where ice is at least 0.40–0.50 m thick, and treat ice regions below 0.40–0.50 m thickness with caution.

1 Introduction

It is well known that Arctic sea ice is experiencing rapid changes in areal extent (Stroeve et al. 2012; Stroeve and Notz 2018), thickness (Lang et al. 2017; Rothrock et al. 1999), and volume (Laxon et al. 2013) at an accelerating rate (Stroeve et al. 2007). Climate models universally agree that high-latitude sea ice will decline throughout the twenty-first century due to rising greenhouse gas concentrations (Zhang and Walsh 2006) but these models also continue to underestimate the observed sea ice decline (Stroeve et al. 2007, 2012; Vaughan et al. 2013). While sea ice extent (edge of ice concentration exceeding 15%) is the conventional indicator of interannual variability in Arctic sea ice conditions, changes in sea ice thickness are demonstrably harder to quantify, complicating modeling efforts (Budikova 2009; Kattsov et al. 2010; Notz 2012; Stroeve

et al. 2014; Wadhams 2012). Vulnerable, thinner first-year ice now dominates the sea ice cover (Maslanik et al. 2011), comprising approximately 70% of Arctic sea ice coverage in March 2019, compared to 35–50% in any March in the 1980s (Perovich et al. 2019). The loss of the thickest multiyear ice extends into the Central Arctic Ocean, where ice previously remained thick enough to persist throughout the summer melt season (Maslanik et al. 2011). Simulations from the recent 6th phase of the Coupled Model Intercomparison Project (CMIP6) estimate that the Arctic Ocean will be practically ice-free, defined as sea ice extent below 1×10^6 km^2, for the first time in September before mid-twenty-first century (SIMIP 2020).

During the cold season, sea ice acts as an efficient thermal insulator between the warm ocean surface and the relatively cooler surface atmospheric boundary layer (Burt et al. 2016; Hines et al. 2015; Seo and Yang 2013) by limiting the amount of energy that passes through the ice (Screen et al. 2013). Sea ice growth, especially for ice below 1.0 m thickness, is inherently tied to a linear temperature gradient between the relatively warmer ocean and the cooler atmosphere above it, and thus the number of freezing-degree days (e.g., Lebedev 1938). Multi-year ice of several meter thickness does not follow a linear thermodynamic growth

✉ Victoria L. Ford
victoriaford@tamu.edu

1 Climate Science Lab, Department of Geography, Texas A&M University, College Station, USA

2 Department of Atmospheric Sciences, Texas A&M University, College Station, USA

pattern. The growth rate between 0.1 and 1.0 m ice thickness decreases by almost an order of magnitude, as the inherent negative feedback of ice growth itself slows further growth and the temperature gradient weakens. Net heat input to the atmosphere is thus primarily determined by the rate at which turbulent heat is transferred from the surface upwards (Serreze and Barry 2014). However, turbulent and conductive energy exchange between the Arctic Ocean and atmosphere, through the sea ice pack, is expected to increase with a thinner overlying ice cover (Maykut 1978). Using a simple heat transport model, (Maykut 1978) found that cold-season heat exchange over 0.0–0.40 m ice thickness is 1–2 times larger than that over perennial ice. Thus, heat losses over thin ice can be critical in the overall Arctic surface energy balance. As Arctic sea ice transitions into a thinner first-year or seasonal cover, it has been suggested that changes in ice thickness may produce significant responses in the atmospheric boundary layer (Gerdes 2006), observable as early in the melt season as spring (Serreze et al. 2009). The magnitude, location, and long-term local and remote impacts of such responses are frequently discussed in the literature (e.g., Screen et al. 2013; Vihma 2014), although the sea ice thickness at which an atmospheric response occurs has not been determined.

In this study, our aim is thus to determine the thickness threshold below which the insulating effect of sea ice is negligible, and to calculate the proportion of total sea ice that falls below the threshold throughout the twentieth and twenty-first century. While the insulating effect of sea ice is well known (e.g., Maykut 1978; Serreze and Barry 2011), the new and unique contribution of this study is to quantify the actual threshold and the area of sea ice that exceeds it. To do so, we simulate the atmospheric response to sea-ice thickness, focusing on the atmospheric boundary layer. We use a series of idealized monthly regional model sensitivity experiments during periods of sea ice freeze-up (October), in the peak of winter (January), and during ice melt (April). The summer period is intentionally not considered, as the complexity of surface air-sea interactions and feedback mechanisms at this time are complicated by a rapidly changing sea ice area boundary. We specifically design a series of sensitivity case-study simulations around prescribed sea ice thicknesses to determine at which thickness we detect a significant response in the overlying atmosphere. We then calculate the proportion of sea ice area below the threshold throughout the twentieth century based on historical observations, and also apply the threshold to twenty-first century projections of sea ice thickness. We intentionally neglect other important physical aspects of interactions between ice cover and the atmosphere, such as fractional ice cover and albedo feedback effects. As such, we do not intend to suggest a replacement for more complicated, coupled, physics-based

parameterizations—rather we seek to isolate the role of ice thickness in an idealized simulation configuration.

2 Data and methods

2.1 Experiment design

A series of 42 idealized sensitivity simulations (14 simulations per season) with spatially-uniform sea ice thicknesses and areas were conducted using the Weather Research and Forecasting model (WRF, v3.9.1) for mid-autumn (sea ice growth), mid-winter (limited growth and/or melt), and mid-spring (sea ice melt, post climatological March sea ice peak). Initial and boundary conditions were forced by ERA-Interim atmospheric reanalysis, available every six hours at 0.5° spatial resolution on 32 pressure levels (Dee et al. 2011) for October 1999, January 2000, and April 2000. These specific months were selected to represent typical monthly sea ice conditions based on the National Snow and Ice Data Center (NSIDC) Sea Ice Index climatological 1981–2010 median (Fetterer et al. 2017), instead of focusing on anomalous sea ice conditions (e.g., the months of record minimum sea ice extent). Respectively, sea ice conditions were 1.1% above, 1.4% below, and 0.8% below the median sea ice extent in October 1999, January 2000, and April 2000.

Simulations were conducted on a 220×220 polar stereographic grid with 9-km horizontal grid spacing and focused on the Central Arctic Ocean, as well as the northern Greenland-Iceland-Norwegian and Barents Seas (Supplementary Fig. 1), so as to highlight the influence of sea ice thickness on the North Atlantic marginal sea ice edge. The first 12 h of each simulation were disregarded as model spin-up. Specific physical parameterizations optimal for the high-latitude environment were used in simulation design, and include the Noah land surface model (Chen and Dudhia 2001), which uses four subsurface layers of identical thickness to represent sea ice thickness. Heat fluxes through the sea ice and snow layer are determined by the distance between the top of the snow layer and the midpoint temperature of the top subsurface thickness layer (Hines et al. 2015). The Grell–Freitas (Grell and Freitas 2014) and two-moment Morrison schemes (Morrison et al. 2005) were used for cumulus parametrization and cloud microphysics, respectively. The Rapid Radiative Transfer Model (Clough et al. 2005) was used for both longwave and shortwave radiation. Similar to other Arctic sea ice studies (e.g., Hines and Bromwich 2016; Hines et al. 2015) we use the Mellor-Yamada-Nakanishi Niino level 2.5 scheme (MYNN 2.5; Nakanishi and Niino 2006) for the atmospheric boundary and corresponding atmospheric surface layers. All simulations have 40 vertical levels, reaching from the surface to 10 hPa, with the lowest four layers representing the planetary boundary layer over the ocean. Other

specifications include sea ice albedo set at 0.82 (Hines et al. 2015) for all simulations, as all runs were prior to the onset of snow melt (Perovich et al. 2002). A fractional sea ice concentration was not implemented, as our focus is to determine the influence of sea ice thickness on the atmosphere. Sea surface temperatures were -1.8 °C beneath the sea ice. Snow depth on sea ice was bounded between 0.001 and 1 m.

2.2 Sea ice thickness threshold

In each season, spatially uniform prescribed sea ice thickness was simulated at 0.05, 0.25, 0.50, 0.75, 1.0, and 2.0 m, with finer 0.05 m runs between 0.25 and 0.75 m. We include a 2.0 m sea ice thickness simulation to appropriately reflect mean sea ice thickness conditions in the historical period, while primarily focusing on the sensitivity of ice thickness below 1.0 m under future thinning conditions. We use the lowest sea ice thickness simulation of 0.05 m to represent open ocean conditions within the Arctic sea ice domain. Statistically significant atmospheric differences at the 95% confidence level were calculated at each grid point using a two-tailed independent-samples t-test assuming equal variance in atmospheric variables between the ice-free simulation and above each ice thickness level. We applied this process for several atmospheric boundary layer variables—2-m surface air temperature, sensible and latent heat flux, planetary boundary layer height, and lifting condensation level height—with a Bonferroni correction to account for multiple comparisons and reduce the likelihood of type I (false positive) errors. We then calculate the percentage of the total sea ice-covered region above which statistically significant differences in atmospheric variables occur. For example, if there is a statistically significant difference in sensible heat flux in the 0.35 m run relative to ice-free conditions above an 8×10^6 km^2 area, this corresponds to significant atmospheric differences occurring above 57% of the total 14×10^6 km^2 ice-covered domain. The percent change between subsequent simulations is then plotted for all runs, using the formula: percent change = [(final state − initial state)/initial state] × 100%.

Numerically, this translates to a large percentage of statistically significant differences between the atmosphere above the thicker sea ice (i.e., 1 m, 2 m) runs and above ice-free conditions, and a small percentage of statistically significant atmospheric differences between thinner (i.e., 0.25 m, 0.30 m) ice and ice-free conditions (not shown). For the autumn simulations, we always consider the initial state to be the lower ice thicknesses, and the final state the larger ice thicknesses. Thus, we expect a small area proportion (few significant atmospheric differences) increasing to a large area proportion (many significant atmospheric differences). In spring, we determine percent change with the opposite physical response; an initial state of simulated large

ice thicknesses and a final state of small ice thicknesses. This results in a transition from a large area proportion with a significant atmospheric response to a small area proportion. For winter, we apply the same interpretation as for spring, because sea ice conditions have been well documented to decline at this time (Cavalieri and Parkinson 2012; Vihma 2014). It should be noted that our methodological design does not simulate growing or melting sea ice, but rather we determine atmospheric differences above uniform sea ice layers of prescribed thicknesses. Based on the resulting line plots of percent changes for the 42 simulations, we expect there to be a transition point in prescribed ice thickness where a discernible switch in the percent of significant atmospheric differences occurs in each of the three seasons. This transition point will indicate the threshold at which sea ice is so thin that it becomes effectively negligible from an atmospheric boundary layer perspective.

2.3 Applying threshold to historical observations and projections

We next apply the sea ice thickness threshold determined from our simulations to the newly released Pan-Arctic Ice Ocean Modeling and Assimilation System for the twentieth century (PIOMAS-20C) (Schweiger et al. 2011, 2019) sea ice thickness reanalysis and recalculate historical sea ice observations to determine an "effective" insulating sea ice area. Thus, we calculate the historical coverage of areas where ice is sufficiently thick to statistically significantly reduce ocean–atmosphere energy exchange. Sea ice below the threshold no longer acts as an insulating layer between the ocean and the atmosphere, and is treated as a region of non-insulating sea ice coverage. Uncertainties in PIOMAS-20C and its predecessor, standard PIOMAS, are of similar magnitude to observed satellite estimates (Labe et al. 2018; Laxon et al. 2013), despite the difference in their atmospheric forcing. PIOMAS-20C reconstructs a 110-years record of Arctic sea ice thickness and volume using ERA-20C atmospheric data for 1901–2010 and reports sea ice volumes generally larger than standard PIOMAS between 1979 and 2010 (Schweiger et al. 2019). Ice thickness biases in the early 1980s are smaller (-0.03 m) in PIOMAS-20C than standard PIOMAS (-0.61 m) when compared to U.S. submarine observations, indicating that PIOMAS-20C ice thickness may more accurately reflect ice thickness than standard PIOMAS.

Lastly, we apply the ice thickness threshold to the CMIP6 shared socio-economic pathways (SSP) 1–2.6, 2–4.5, and 5–8.5 emissions scenarios to estimate twenty-first century sea ice thickness conditions. Of the CMIP6 models recommended by SIMIP (2020), we use the first ensemble members of ACCESS-CM2, GFDL-ESM4, MPI-ESM1-2-h, MPI-ESM1-2-LR, MRI-ESM2-0, and NorESM2-MM in

each SSP emissions scenario. This subset of CMIP6 models is able to simulate realistic sea ice loss and simultaneous plausible changes in cumulative anthropogenic CO_2 emissions over time, and output sea ice thickness. We also assess the relationship between Arctic sea ice thickness to historical (Friedlingstein et al. 2019) and future cumulative anthropogenic CO_2 emissions (Riahi et al. 2017).

3 Results

3.1 Atmospheric response to sea ice changes

As sea ice thickness decreases, heat fluxes from the warmer ocean increase to the relatively cooler atmosphere, prompting increases in simulated surface air temperature (Fig. 1). During mid-autumn freeze-up conditions (Fig. 1a), domain-averaged surface air temperatures indicate less than 3.5 K difference between ice-free conditions and 2 m thick sea ice. Over the course of the month, surface air temperature across all runs consistently drop by approximately 10 K. Mechanistically, we demonstrate that as sea ice freezes and thickness increases, surface air temperatures decrease as oceanic thermal energy is prevented from reaching and interacting with the surface boundary layer. Winter variations in surface air temperatures range between 3 and 8 K difference between ice thickness simulations (Fig. 1b), with differences increasing with time as the observed surface air temperature decreases (dashed black line). Temperature differences during the spring melt period ranged 4.5–7 K, with differences between simulated ice thicknesses decreasing as temperatures increased. In late winter and early spring, we note that the surface air temperature difference between 1 and 2 m ice is approximately equal to the differences between the thinner quarter-meter ice runs. This difference can be as high as a 1 K difference as ice thins. In other words, an equivalent

amount of surface temperature response occurs when ice thins from 2 to 1 m as it does between 0.50 and 0.25 m. This enhanced response in the surface air temperature field may be related to the physical ice growth/melt process itself, where greater amounts of energy pass through the ice layer when ice is thinner. Simulated air temperatures follow the observed surface air temperature pattern (Fig. 1, dashed black lines) reasonably well in each season, providing confidence in the simulated response.

With higher surface air temperatures, an increase in the local planetary boundary layer (PBL) height is expected. Enhanced latent heat flux in areas that transition from ice-covered to ice-free increase the relative surface humidity, lower the lifting condensation level (LCL), and increase low-level cloud coverage. Based on the range in vertical temperature profiles between simulations (Supplementary Fig. 2), we utilize five variables—surface air temperature, sensible and latent heat fluxes, and PBL and LCL heights—as useful parameters to diagnose the atmospheric response to varying sea ice thicknesses. We do not use surface pressure, as variations between simulations were too small (Gerdes 2006; Hines et al. 2015) and not statistically significant.

3.2 Establishing a sea ice thickness threshold

Based on the five variables, we calculate the percent area differences in the atmospheric response between each of the 0.25–2.0 m sea ice simulations and the ice-free simulation. The progression of differences in percent area change between model simulations for all five variables in each season is roughly exponential, suggesting a transition in the physical response (Fig. 2). Interpreting these percent area changes, we identify three stages within the atmospheric response to varying sea ice thickness: stable decline, a transitional period, followed by a rapid decline. In winter and spring, there is a small but gradual decrease in the percent
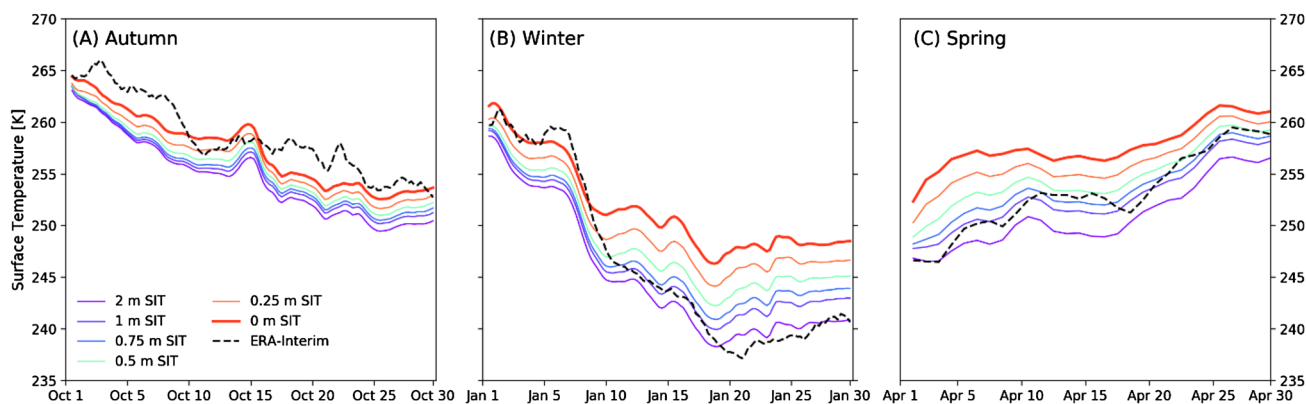

Fig. 1 Domain-averaged surface air temperatures in sea ice thickness simulations (colored lines), and observations (black dashed line) in **a** autumn, **b** winter, **c** and spring. The diurnal signal was removed from the spring surface air temperatures
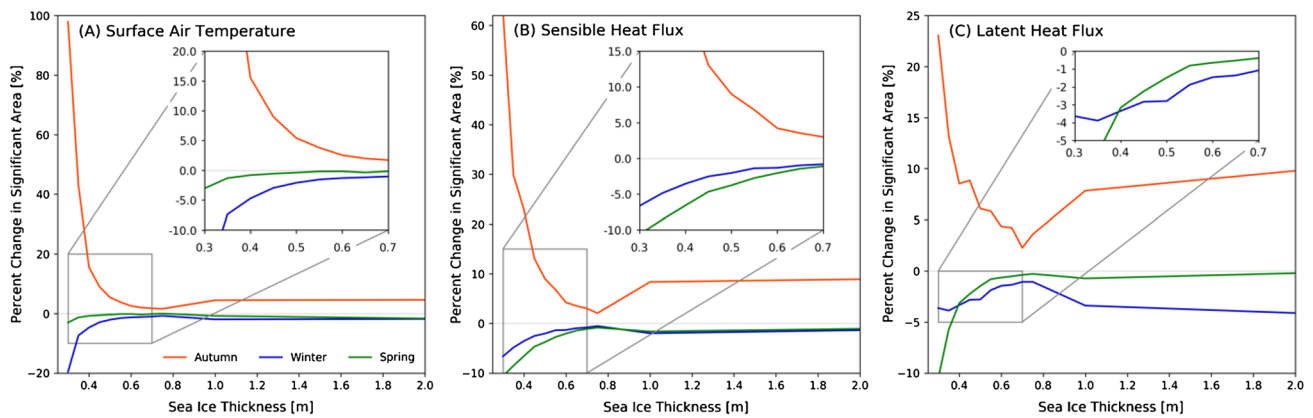
Fig. 2 Seasonal percent change in statistically significant area differences between sea ice thickness simulations and no-ice conditions for **a** surface air temperature, **b** sensible heat flux, and **c** latent heat flux

area above which significant differences in atmospheric variables occur (i.e., above 1 m). This gradual decline corresponds to sufficiently thick ice, with negligible to minimal statistical differences in the atmospheric response (of any variable) relative to ice that is 1 or 2 m thick. This is followed by a transition point, where the percent of areas with significant atmospheric differences experiences greater change as the ice thickness varies. In autumn, a change from a small percent area to a large percent area with significant atmospheric differences is observed, and the inverse change in winter and spring. We observe the transitional period in all seasons and variables at ice thicknesses between 0.40 and 0.50 m. This result is consistent with the energy exchange estimates for thin ice below 0.40 m reported by Maykut (1978). At ice thicknesses below 0.40 m, the percent area of significant atmospheric differences rapidly declines in winter and spring, indicating that at very thin ice conditions there are no statistical atmospheric differences between ice-free and thin ice states. A similar pattern occurs in the autumn freeze-up period, as ice grows from very thin ice into a thicker layer. From very thin ice up to 0.40 m, we observe a rapid decline in the percent ice area with significant differences in atmospheric variables. As ice thickness increases above 0.50 m in autumn, there is very little difference in the percent area of significant atmospheric response. Surface air temperature (Fig. 2a) and sensible heat flux (Fig. 2b) exhibit the largest magnitude of changes in area percentage of significant differences, as a thermal response is more readily transferred through a sufficiently thin ice layer than moisture. While the latent heat flux (Fig. 2c) patterns show much weaker changes in the percent of area with significant differences, the same pattern emerges. To maintain uniform sea ice coverage, we do not simulate sea ice growth/melt in our sensitivity simulations, however, in reality, turbulent latent heat release leads to ice growth, maintaining a strong ocean-to-atmosphere temperature gradient, and thus

an upward flux through the sea ice. The PBL height and LCL height responses also follow this exponential change (Supplementary Fig. 3). The increases in the percent area change with ice thicknesses greater than 0.75 m in autumn, and similar decreases in winter and spring, may be an artifact of the relatively fewer number of sensitivity simulations for thicknesses greater than 0.75 m, and not a meaningful physical response in the system.

Based on the consistent exponential pattern of percent area differences in statistically significant atmospheric response differences to varying ice thicknesses, we determine a sea ice thickness threshold exists and corresponds to the transition zone between 0.40 to 0.50 m. A quantitative analysis of the first derivative of each of these plots (not shown) confirms the transition and hence threshold between 0.40 and 0.50 m.

To quantify the magnitude of energy exchange occurring in sea ice areas below the ice thickness threshold, we characterize the surface air temperature, sensible and latent heat fluxes, and PBL and LCL height response in each season. To do this, the atmospheric variables corresponding to the 0.40, 0.45, and 0.50 m ice thickness simulations are averaged to represent the threshold thickness conditions, and are compared to the atmospheric variables corresponding to ice-free conditions. In autumn (Fig. 3, top row), when the ocean and atmosphere are still highly coupled, positive surface air temperature differences dominate throughout the domain, with an average difference of 2.1 K between the threshold level and ice-free conditions (Supplementary Table 1). There is a discernible gradient of positive differences across the Arctic Ocean: the weakest positive differences of 0.3 K were noted in the eastern Arctic near the sea ice edge, while the largest positive differences of 3 K off the eastern Greenland coast and throughout the central Arctic. Sensible and latent heat fluxes also exhibit positive differences, with patterns coupled to the surface air temperature spatial response. Sensible heat
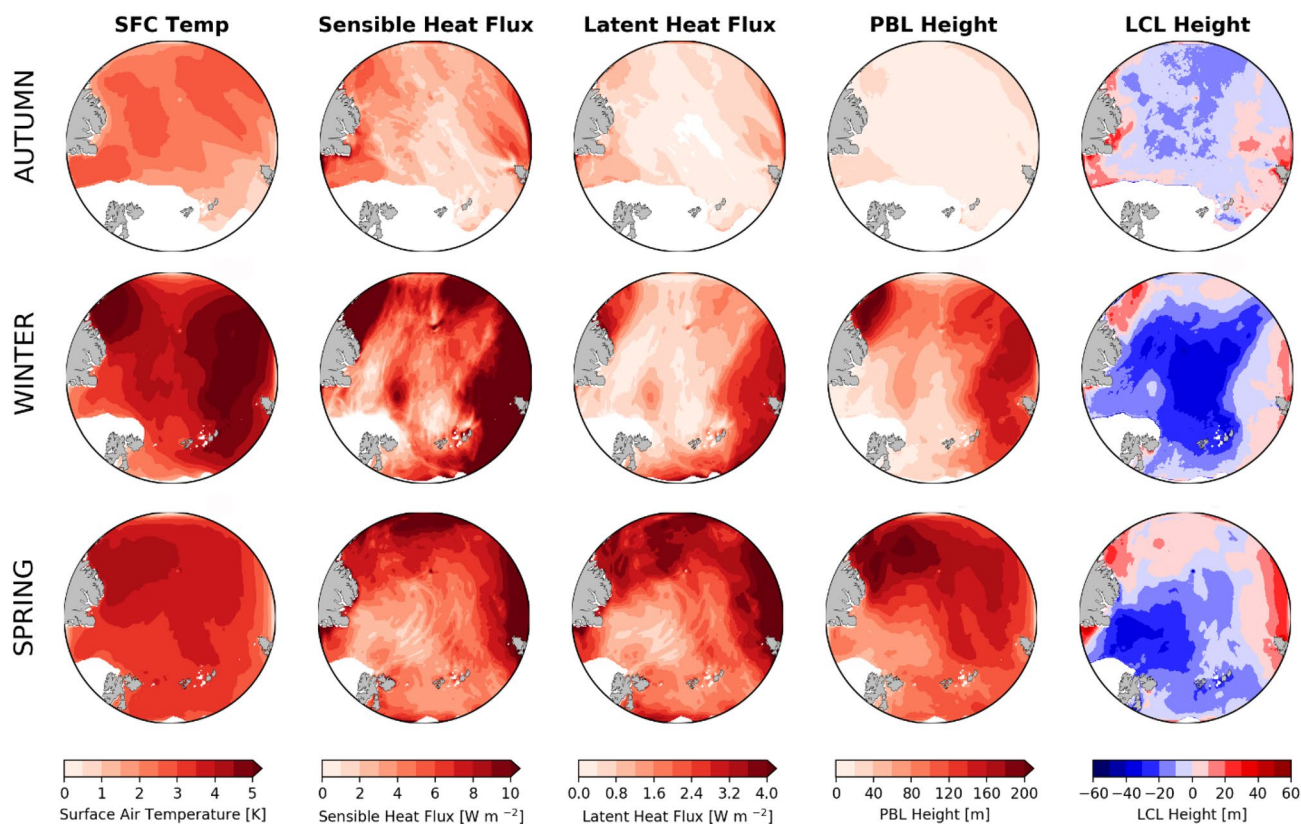
Fig. 3 Monthly mean difference in surface atmospheric properties between sea ice thickness threshold and no-ice conditions for autumn (top row), winter (center row), and spring (bottom row). Scales consistent for respective column

flux differences exceeded 10 W m^{-2} surrounding the Greenland coastline. Weaker, but positive sensible heat flux differences ranging between 1 and 4 W m^{-2} dominate the central Arctic, with an average difference of 3.55 W m^{-2}. Latent heat flux differences were weaker than the sensible heat flux response, with differences primarily below 1 W m^{-2} throughout the domain. Autumn PBL height exhibits a fairly weak response, with a positive average increase of 15 m, with regions approaching 60 m differences near coastlines. LCL height differences are largely constrained to decreases in the Central Arctic Ocean with a mean -2 m decline, and weak positive differences close to land which may result from local atmospheric conditions over these land regions.

As expected, the largest response for most variables is evident in winter, when the temperature difference between ocean and atmosphere is largest (Fig. 3, middle row). Across the Arctic Ocean, a bimodal spatial pattern is identified, with the strongest positive differences centered over the eastern Arctic, in the vicinity of the Kara and Laptev Seas. A smaller region just north of Greenland also exhibits a strong positive response. Surface air temperature differences in these two regions exceed 4–5 K, with an average of 3.85 K across the entire domain (Supplementary Table 1). Smaller, positive differences of 1–3 K near the sea ice edge

in the northern Barents Sea. This bimodal pattern is also seen in the heat fluxes, likely due to the strong surface air temperature response there. Sensible heat flux differences exceeded 10 W m^{-2} in these two regions. While not as dominant as the sensible heat flux differences, latent heat flux differences near 6 W m^{-2} are seen at the domain periphery, but average near 1.56 W m^{-2} throughout the domain. A strong response is concurrently seen in PBL height of increases more than 150 m, primarily in the same spatial bimodal pattern between the eastern and western Arctic. Average PBL height differences in the central Arctic ranged between 20 and 100 m. Height of the LCL exhibited the strongest negative differences in winter, both in depth of response and spatial extent, with differences throughout the central basin exceeding -40 m. Weaker positive differences of 10 m similarly occurred along the domain edge.

Spring atmospheric differences between the threshold and ice-free conditions also show a strong response in the lower atmosphere (Fig. 3, bottom row), with surface air temperature differences above 3 K throughout the entire domain (Supplementary Table 1). Temperature differences shifted from a bimodal pattern into a more focused center north of Greenland, where differences were greater than 4 K. Sensible heat flux differences in spring were positive everywhere,

reaching up to 32 W m^{-2} in the northern Kara Sea. Larger positive sensible heat flux differences occur more towards the Pacific side of the Arctic, likely due to very thin ice at the end of the winter growth period. Latent heat flux and PBL height differences are strongest in spring throughout the domain. Latent heat flux differences exceed 4 W m^{-2}, coincident with the strongest sensible heat flux differences in the Kara Sea and towards the Pacific. Weaker positive latent heat flux differences were centered between northeastern Greenland and Svalbard, with differences just above 0.5 W m^{-2}. The pattern of PBL height differences resembles the surface air temperature differences, with the strongest response north of Greenland where differences exceed 200 m. The mean PBL height difference throughout the domain was greater than 120 m, indicating large changes in PBL height response between ice-free conditions and ice at the threshold. Differences in the spring LCL height exhibited strong negative differences greater than -20 m near the sea ice margin off Greenland's northeastern coast. In general, the energy exchange in regions where ice thickness is below the threshold of 0.40–0.50 m is as follows: surface air temperature differences exceed 2 K, despite ice presence in areas where ice thickness is below the threshold. The turbulent heat fluxes are dominated by the sensible heat flux response, but are positive everywhere. Height of the PBL is strongly coupled to the surface air temperature pattern, with strong seasonally-dependent differences of more than 200 m. The LCL height generally decreases over the thin sea ice areas, with the strongest negative differences seen in the central Arctic Ocean, away from land influence, near -20 to -40 m.

3.3 Historical ice area below the threshold

As expected, sea ice below the threshold, which does not act as an insulating layer between the ocean and the atmosphere, is mostly located at the sea ice periphery (Fig. 4). Autumn exhibits the largest areas of non-insulating sea ice, when the Arctic Ocean begins to refreeze and new seasonal ice has not yet reached the thickness threshold (Fig. 4a). Notable regions are northern Baffin Bay and along the Arctic Ocean basin edges where new sea ice forms. Although we did not consider a fractional ice cover, a large system of polynyas has been reported to form in these regions in winter and spring (Morales Maqueda et al. 2004), where the generation of very thin ice, sub-thickness threshold, can contribute to the warming signal simulated at this time. Winter and spring non-insulating sea ice areas are primarily along the Atlantic sea ice margin (Fig. 4b, d). Focusing on the September 2007 sea ice minimum (Fig. 4e) as an example, much of the non-insulating sea ice was predominantly located adjacent to the Greenland and Canadian Arctic Archipelago coastlines.

Throughout the twentieth century, non-insulating sea ice area accounts for 6–12% of the reported total sea ice area when using PIOMAS-20C (Fig. 4c). During the first half of the twentieth century the average percent ice area below the thickness threshold was 7–10%, followed by a decline until approximately 1980. This decline may reflect internal variability in the climate system, and we thus focus on the increasing trend from 1980 onwards. This trend corresponds to increasing amounts of non-insulative sea ice, at a time when in-situ observations indicate declining sea ice thicknesses. Distinct peaks when the non-insulative sea ice area is larger than average correspond to notable sea ice minimum events, such as the Early Twentieth Century Warming period (Schweiger et al. 2019), the Great Salinity Anomaly of the late 1960s–early 1970s (Häkkinen 1993), and the 2007 record sea ice minimum (PIOMAS-20C ends in 2010, therefore the 2012 record minimum is not included here). To distinguish between ice melt or ice growth, the seasonal contributions towards the annual percentages (Fig. 4f) indicate that autumn consistently exhibits the largest amount of non-insulating sea ice areas throughout the twentieth century. The autumn percent of area below the threshold ranges between 9 and 18% of the PIOMAS-20C total sea ice area, which can be physically attributed to the amount of new seasonal growth post-ice minimum. Also noteworthy is the percentage of autumn ice below the threshold post-1980, which increases from 10 to 15% of the total sea ice cover, and may be the dominant contributor to the annual increase (Fig. 4c). Summer ranges between 5 and 14%, as areas of thin ice melt each year prior to the September ice minimum. As ice grows beyond the thickness threshold throughout winter and at the March ice maximum, the percent of non-insulating sea ice areas in winter and spring were fairly uniform throughout the twentieth century, with 5–9% and 3–7% of the PIOMAS-20C total sea ice area, respectively.

Similar percentages are found compared to the reported NSIDC total sea ice area for 1979–2010 (Table 1). A seasonal cycle of ice area below the threshold is evident between the ice growth season (October through March) and ice melt period (April through September). In the cold season, non-insulating sea ice area increases in magnitude and variability, accounting for 4–14% of the total sea ice area reported by the NSIDC. Cold season non-insulating sea ice areas are typically above 0.6×10^6 km^2 with monthly means between 0.72 and 0.97×10^6 km^2 (Table 1). We estimate that an average of approximately 10–14% of the total sea ice area, or 1×10^6 km^2, is below the thickness threshold in October and November, and can be as high as 1.45×10^6 km^2. Post-ice maximum in March, the magnitude and variability of non-insulating ice area is smaller, between 4 and 9% (between 0.39 and 0.59×10^6 km^2), and as low as 0.20×10^6 km^2. Even the lowest amount of non-insulating sea ice area
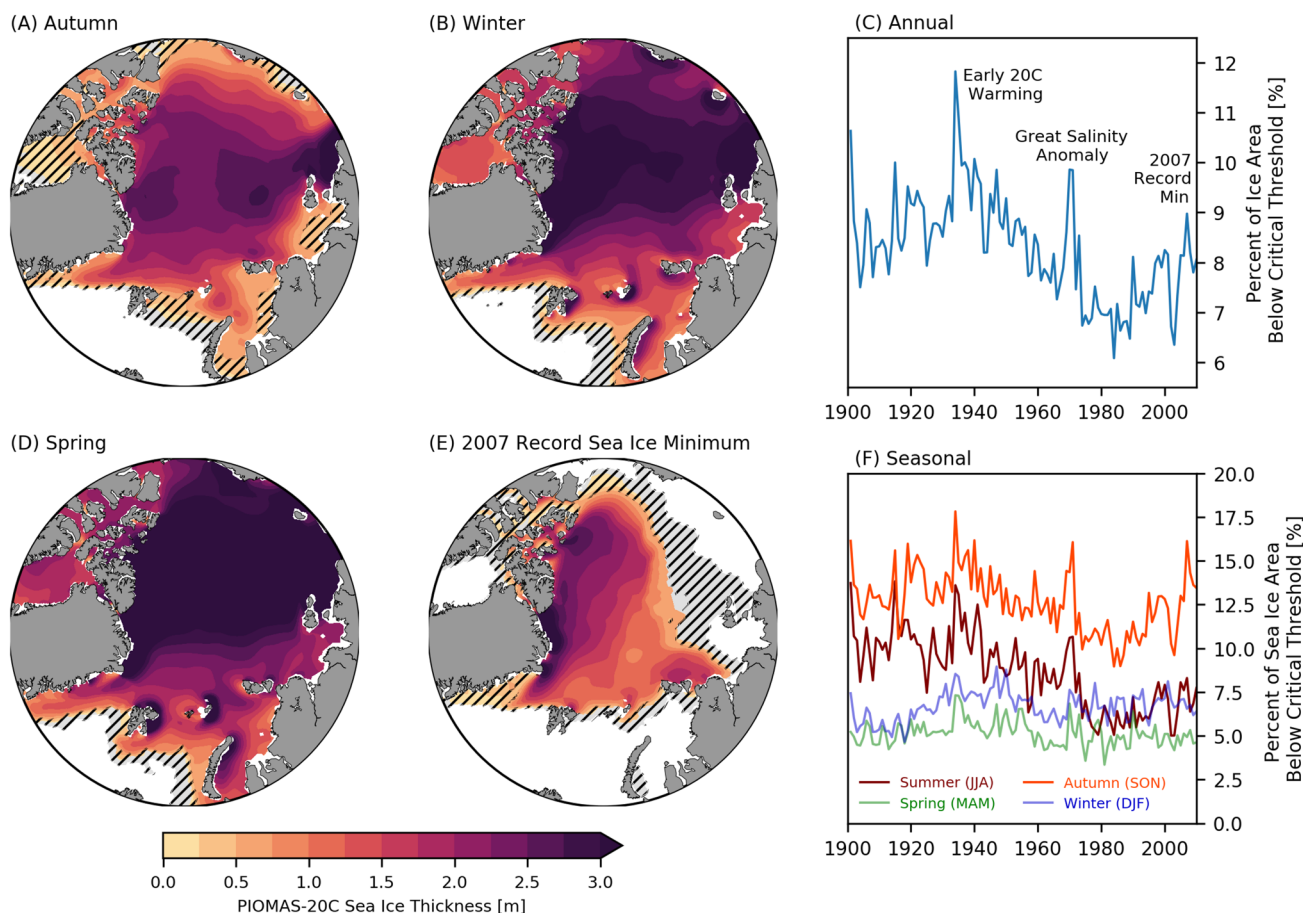
Fig. 4 Sea ice thickness across the Arctic Ocean from the PIOMAS-20C reanalysis for **a** autumn (October 1999), **b** winter (January 2000), **d** spring (April 2000), and **e** the 2007 record sea ice minimum (September 2007). Sea ice area below the sea ice thickness threshold is hatched, and areas where sea ice thickness coincides with sea ice concentration below 0.15 are shaded light grey. **c** Annual and **f** seasonal contributions to the percent of total sea ice area below the sea ice thickness threshold

Table 1 Comparison of monthly 1979–2010 observed total sea ice area (NSIDC) and calculated sea ice area below ice thickness threshold

	January	February	March	April	May	June
NSIDC total area (10^6 km^2)	11.65–13.18 (12.29)	12.26–13.77 (13.08)	12.52–13.90 (13.19)	11.83–13.18 (12.54)	10.47–11.66 (11.14)	8.21–9.95 (9.18)
Area below threshold (10^6 km^2)	0.63–1.02 (0.82)	0.64–1.1 (0.80)	0.47–0.97 (0.72)	0.35–0.79 (0.59)	0.38–0.61 (0.50)	0.27–0.54 (0.40)
Percent of total (%)	6.7	6.1	5.4	4.7	4.5	4.4
	July	August	September	October	November	December
NSIDC total area (10^6 km^2)	5.13–7.44 (6.44)	3.19–5.73 (4.74)	2.82–5.64 (4.45)	4.33–7.74 (6.46)	8.06–9.91 (8.94)	10.17–11.99 (10.89)
Area below threshold (10^6 km^2)	0.32–0.55 (0.43)	0.20–0.56 (0.39)	0.22–0.63 (0.41)	0.60–1.23 (0.91)	0.58–1.43 (0.97)	0.61–0.98 (0.81)
Percent of total (%)	6.7	8.2	9.3	14.1	10.9	7.5

Ranges provided as minimum and maximum values, with means in parenthesis. Percentages of mean ice area below the threshold of observed mean total ice area are also provided

in any month is still at least 4% of the reported total sea ice area.

3.4 Future ice area below the threshold

Historical and twenty-first century projections for cumulative CO_2 emissions under SSPs 1–2.6, 2–4.5, and 5–8.5 emission scenarios are calculated using a subset of CMIP6 models that realistically simulate sea ice decline (SIMIP 2020). The evolution of cumulative CO_2 emissions exhibits a complex relationship with mean sea ice thickness in March, September, and at an annual scale (Fig. 5a–c), more so than the strong linear correlation between sea ice area and cumulative CO_2 emissions reported by Stroeve and Notz (2018) and SIMIP (2020).

In March (Fig. 5a), mean sea ice thickness is not projected to fall below the thickness threshold under future cumulative CO_2 emission conditions in any SSP scenario until emissions are well above current CO_2 emission levels. For September, the multi-model ensemble mean for SSP5-8.5 conditions does reach the thickness threshold, but at high cumulative CO_2 emissions near 10,000 Gt. The September trend (Fig. 5b) does exhibit more variability than the March and annual (Fig. 5c) trends, and so we treat September with equal caution. The annual trend is similar to that of March, with the multi-model ensemble mean cumulative

CO_2 emissions not crossing the thickness threshold. We do note that one individual ensemble member does cross the thickness threshold under SSP2-4.5 and SSP5-8.5 future CO_2 emissions at approximately 5,000 Gt, and two individual model members at 7500 Gt in SSP5-8.5 future CO_2 emissions (Supplementary Fig. 4). This may be due to those individual models having lower initial sea ice thickness compared to others.

Throughout time (Fig. 5d–f), future projected mean sea ice thickness does not reach the thickness threshold before the end of the century, except in September very near 2100. Under future SSP1-2.6 and SSP2-4.5 conditions, mean sea ice thickness tails off near 1.0 m thickness, while future SSP5-8.5 estimates of sea ice thickness however around 0.65 m in March and 0.25 m in September. However, by discerning the declining trend in thickness observations in all three time periods, mean sea ice thickness is projected to be below the thickness threshold before 2050, and as early as the mid-2020s in September. As is well documented (SIMIP 2020; Stroeve et al. 2007, 2012; Vaughan et al. 2013), global coupled models routinely fail to capture the same decline as the observations.

We note that the loss of sea ice thickness is more similar to changes in ice volume, than those of ice area, which may explain the lack of a more direct linear relationship between cumulative CO_2 emissions and ice thickness. As the sea ice
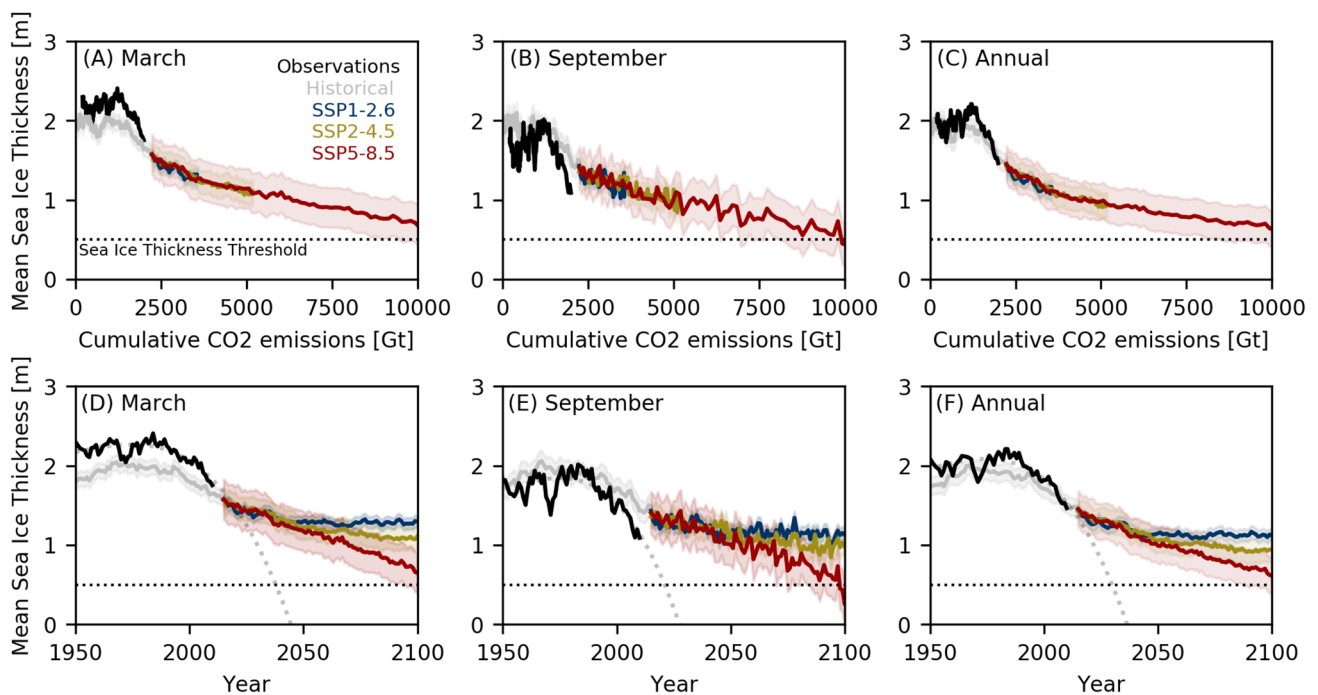

Fig. 5 Evolution of Arctic sea ice thickness over the historical period (1950–2019) and corresponding three scenario projections for March (**a, d**), September (**b, e**), and annual (**c, f**) as a function of cumulative CO_2 emissions (**a–c**) and time for CMIP6 models (**d–f**). Shading represents ± 1 standard deviation around the multi-model ensemble means (thick line). Cubic quadrilateral trends (dashed lines) are fitted to decline in ice thickness observations. Sea ice thickness threshold at 0.50 m is demarked

cover continues to shrink in areal extent, the transition to thinner ice should be also carefully considered. Obviously, while CO_2 is an important driver of changes to the Arctic ice system, it is not the only external cause contributing to sea ice loss.

3.5 Caveats and additional considerations

The determination of a sea ice thickness threshold and the resulting atmospheric response may be sensitive to the choice of atmospheric forcing and planetary boundary layer scheme. To assess sensitivity to our choice of atmospheric forcing, we performed an additional simulation in each season utilizing CFSRv1 reanalysis, instead of ERA-Interim. We find statistically significant differences between simulations at the same thickness level with differing atmospheric forcing data, suggesting that the choice of atmospheric forcing data does matter. While there are shortcomings in ERA-Interim, namely a warm wintertime temperature bias (Simmons and Poli 2015), Graham et al. (2019) determine it to be the most realistic reanalysis for Arctic sea ice studies during our time period of interest. To address sensitivity to the planetary boundary layer scheme, we conducted an additional simulation in each season with a uniform prescribed sea ice thickness of 0.50 m, keeping all simulation settings the same, except for the use of the Mellor-Yamada-Janjić PBL scheme (MYJ; Janjić 2001) instead of MYNN 2.5. We find no statistically significant differences between these two PBL schemes in our selected atmospheric parameters in any season, except for the wintertime sensible heat flux, which exhibited a minor (< 15%) difference. Thus, we expect our results and the sea-ice thickness threshold are not sensitive to the choice of PBL scheme.

While not explicitly assessed in this study, we acknowledge that the spatial variation in depth, distribution, and density of a snow depth layer on sea ice can determine whether there is additional ice growth or loss (Webster et al. 2014). There were no discernible differences in snow depth between our simulations (both inter- and intra-seasonal comparisons) that would suggest snow on sea ice to have an appreciable impact on our results. Furthermore, providing our threshold as a range (0.40–0.50 m) rather than one precise thickness value accounts for slight variations from factors such as snow. The choice of a uniform ice thickness layer in our sensitivity study obviously does not simulate the complexities of a realistic heterogenous fractional ice cover. Leads and polynyas create regionally-important avenues for heat conduction and energy exchange to the atmosphere within the ice cover (Taylor et al. 2018), which will increasingly contribute to localized warming with a more fractured future ice cover. Understanding the importance of turbulent energy exchange within a thinning fractional ice cover

is critical for narrowing the inter-model spread for future Arctic amplification.

In our idealized sensitivity study focusing specifically on sea ice thickness, we only present one piece of a much larger and complex climate puzzle. Testing the applicability of this threshold in fully coupled atmosphere–ocean-ice global coupled models would be an interesting future research avenue. Additional complex feedbacks within the Arctic system may have a role in influencing the ice thickness threshold. These include the ice-albedo feedback, which has been found to account for only half of Arctic surface temperature increases, with changes in sea ice thickness and extent accounting for the remainder (Hall 2004); water vapor feedback (Ghatak and Miller 2013) and the importance of clouds in the fall (Kay and Gettelman 2009); and enhanced thinning of ice from downwelling longwave radiation (Burt et al. 2016). These changes and their the mid-latitude remote responses, can only be simulated in a realistic fully-coupled model design.

Finally, we acknowledge the importance of albedo, especially as the Arctic transitions to only seasonal ice cover (e.g., Björk et al. 2012; Curry et al. 1995; Thackeray and Hall 2019). As our intent was to solely assess the sensitivity of ice thickness and ice's ability to conduct or insulate in the context of sensible and latent heat, we intentionally set albedo to a constant value and our results do not assess the importance of sea-ice thickness on surface radiative fluxes.

4 Conclusions

As Arctic sea ice continues to transition from a thick, multi-year ice cover into a thinner seasonal state, basin-wide sea ice areas approach an ice thickness threshold below which sea ice no longer effectively insulates the ocean from the atmosphere. We assessed where sea ice has a negligible impact on surface sensible and latent heat fluxes and the atmospheric boundary layer response based on this ice thickness threshold by delineating between thick ice areas that effectively prevent energy exchange and those non-insulating ice areas that are thin enough to produce a significant response in the lower atmosphere despite ice presence. Using an idealized suite of 42 WRF sensitivity simulations for the Arctic Ocean with varying prescribed uniform sea ice thicknesses, we determined that the change in percent of statistically significant areas in several atmospheric variables between ice-free conditions and various sea ice thicknesses follows an exponential pattern. This pattern displays a consistent transition zone which we assign as our thickness threshold. The threshold, consistently observed in this transition zone based on multiple atmospheric variables and across seasons, is 0.40–0.50 m for Arctic sea ice.

More than 2 K of atmospheric warming occurs above sea ice that is below the threshold, despite ice presence in those areas. We applied this threshold to historical observations over the twentieth century, and found that nearly 4–14% of the reported total sea ice area falls below this thickness threshold, reducing the total sea ice area to only those ice regions that effectively insulate the atmosphere from the relatively warmer ocean. More variability in non-insulating sea ice areas was found in the cold (ice growth) season from October through March during 1979–2010, when approximately $0.72–0.97 \times 10^6$ km^2 of ice was below the thickness threshold. However, non-insulating Arctic sea ice area accounts for as much as 1.45×10^6 km^2, and notable sea ice minimum events and records were even lower than reported, by as much as 10–12% of the total sea ice area. Our results do not offer conclusive evidence on how sea ice thickness may affect the larger overall climate; however, a recent study by Lang et al. (2017) has shown that changes in sea ice thickness can affect the magnitude of Arctic amplification, especially in near-surface winter warming. Thus, our finding that ice below a critical thickness has influence on heat fluxes between the ocean and the atmosphere may provide further context, suggesting that estimates of the true ice extent and therefore its atmospheric feedbacks should focus on ice above or below our thickness threshold.

Using PIOMAS-20C, a cubic fit of the observed sea ice thickness decline indicates mean ice thicknesses will be below the thickness threshold before 2050, and as early as the mid-2020s in September. The CMIP6 multi-model ensemble mean based on three SSP scenarios does not capture this same decline in sea ice thickness. Determination of future projected cumulative anthropogenic CO_2 emissions reveals a non-linear relationship, hinting at the complex influence of increasing emissions on ice thickness losses and should be investigated further. However, as is well documented in the literature, modeling efforts underestimate the decline in sea ice observations.

Applying the thickness threshold in fully coupled climate simulations and assessing the influence of varying parameters such as sea ice concentration and ice feedback realizations may refine the sea ice thickness threshold beyond a range of 0.40–0.50 m. As Arctic sea ice continues to transition into a thinner, more seasonal ice cover, greater amounts of sea ice area are expected to fall below the thickness threshold. The immediate and long-term responses in the atmosphere point towards further additional warming and thermal energy exchange, as large areas of thin ice no longer act as an insulating layer between ocean and atmosphere. Such a threshold may prove critical in assessing future local and remote atmospheric impacts, especially in the autumn freeze-up period, when very thin ice will dominate the sea ice cover. Fully-coupled studies on ocean–atmosphere energy exchanges as they relate to historical and future sea ice area should also consider the importance of sea ice thickness, especially in thinning ice regions where the thermodynamic response is enhanced. Localized areas of sea ice less than 0.40–0.50 m thickness should be considered as non-insulating or conductive in nature, and treated with caution when analyzing the future of an increasingly seasonal sea ice area.

References

Björk G, Stranne C, Borenäs K (2012) The sensitivity of the arctic ocean sea ice thickness and its dependence on the surface Albedo parameterization. J Clim 26:1355–1370. https://doi.org/10.1175/JCLI-D-12-00085.1

Budikova D (2009) Role of Arctic sea ice in global atmospheric circulation: a review. Global Planet Change 68:149–163

Burt MA, Randall DA, Branson MD (2016) Dark warming. J Clim 29:705–719

Cavalieri DJ, Parkinson CL (2012) Arctic sea ice variability and trends, 1979–2010. Cryosphere 6:881

Chen F, Dudhia J (2001) Coupling an advanced land surface–hydrology model with the Penn State–NCAR MM5 modeling system. Part I: model implementation and sensitivity. Mon Weather Rev 129:569–585

Clough SA et al (2005) Atmospheric radiative transfer modeling: a summary of the AER codes. J Quant Spectrosc Radiat Transfer 91:233–244

Curry JA, Schramm JL, Ebert EE (1995) Sea ice-albedo climate feedback mechanism. J Clim 8:240–247

Dee DP et al (2011) The ERA-Interim reanalysis: configuration and performance of the data assimilation system. Q J R Meteorol Soc 137:553–597

Fetterer F, Knowles K, Meier W, Savoie M, Windnagel AK (2017) Sea Ice Index, version 3. Boulder, Colorado

Friedlingstein P et al (2019) Global carbon budget 2019. Earth Syst Sci Data 11:1783–1838. https://doi.org/10.5194/essd-11-1783-2019

Gerdes R (2006) Atmospheric response to changes in Arctic sea ice thickness. Geophys Res Lett 33:1–4. https://doi.org/10.1029/2006GL027146

Ghatak D, Miller J (2013) Implications for Arctic amplification of changes in the strength of the water vapor feedback. J Geophys Res Atmos 118:7569–7578

Graham RM et al (2019) Evaluation of six atmospheric reanalyses over Arctic sea ice from winter to early summer. J Clim 32:4121–4143

Grell GA, Freitas SR (2014) A scale and aerosol aware stochastic convective parameterization for weather and air quality modeling. Atmos Chem Phys 14:5233–5250

Häkkinen S (1993) An Arctic source for the great salinity anomaly: a simulation of the Arctic ice-ocean system for 1955–1975. J Geophys Res Oceans 98:16397–16410

Hall A (2004) The role of surface albedo feedback in climate. J Clim 17:1550–1568

Hines KM, Bromwich DH (2016) Simulation of late summer Arctic clouds during ASCOS with polar WRF. Mon Weather Rev 145:521–541. https://doi.org/10.1175/MWR-D-16-0079.1

Hines KM, Bromwich DH, Bai L, Bitz CM, Powers JG, Manning KW (2015) Sea ice enhancements to Polar WRF. Mon Weather Rev 143:2363–2385

Janjić ZI (2001) Nonsingular implementation of the Mellor-Yamada level 2.5 scheme in the NCEP Meso model Tech Rep 437. http://www.emc.ncep.noaa.gov/officenotes/newernotes/on437.pdf

Kattsov VM et al (2010) Arctic sea-ice change: a grand challenge of climate science. J Glaciol 56:1115–1121

Kay JE, Gettelman A (2009) Cloud influence on and response to seasonal Arctic sea ice loss. J Geophys Res Atmos 114:D18204. https://doi.org/10.1029/2009JD011773

Labe Z, Magnusdottir G, Stern H (2018) Variability of Arctic Sea Ice thickness using PIOMAS and the CESM large ensemble. J Clim 31:3233–3247

Lang A, Yang S, Kaas E (2017) Sea ice thickness and recent Arctic warming. Geophys Res Lett 44:409–418

Laxon SW et al (2013) CryoSat-2 estimates of Arctic sea ice thickness and volume. Geophys Res Lett 40:732–737

Lebedev V (1938) Growth of ice in Arctic rivers and seas and its dependence on negative air temperature. Prob Arktiki 5:9–25

Maslanik J, Stroeve J, Fowler C, Emery W (2011) Distribution and trends in Arctic sea ice age through spring 2011. Geophys Res Lett 38:1–6. https://doi.org/10.1029/2011GL047735

Maykut GA (1978) Energy exchange over young sea ice in the central Arctic. J Geophys Res Oceans 83:3646–3658

Morales Maqueda MA, Willmott AJ, Biggs NRT (2004) Polynya dynamics: a review of observations and modeling. Rev Geophys. https://doi.org/10.1029/2002RG000116

Morrison H, Curry JA, Khvorostyanov VI (2005) A new double-moment microphysics parameterization for application in cloud and climate models. Part I: description. J Atmos Sci 62:1665–1677

Nakanishi M, Niino H (2006) An improved Mellor-Yamada level-3 model: Its numerical stability and application to a regional prediction of advection fog. Bound-Layer Meteorol 119:397–407

Notz D (2012) Challenges in simulating sea ice in earth system models. Wiley Interdiscip Rev Clim Change 3:509–526

Perovich DK et al (2019) Arctic Report Card: Sea Ice. https://arctic.noaa.gov/Report-Card/Report-Card-2019/ArtMID/7916/ArticleID/841/Sea-Ice. Accessed 17 Jan 2020

Perovich DK, Grenfell TC, Light B, Hobbs PV (2002) Seasonal evolution of the albedo of multiyear Arctic sea ice. J Geophys Res Oceans 107:SHE-20

Riahi K et al (2017) The shared socioeconomic pathways and their energy, land use, and greenhouse gas emissions implications: an overview. Global Environ Change 42:153–168

Rothrock DA, Yu Y, Maykut GA (1999) Thinning of the Arctic sea-ice cover. Geophys Res Lett 26:3469–3472

Schweiger A, Lindsay R, Zhang J, Steele M, Stern H (2011) Uncertainty in modeled arctic sea ice volume. J Geophys Res. https://doi.org/10.1029/2011JC007084

Schweiger A, Wood K, Zhang J (2019) Arctic sea ice volume variability over 1901–2010: a model-based reconstruction. J Clim 32:4731–4752

Screen JA, Simmonds I, Deser C, Tomas R (2013) The atmospheric response to three decades of observed Arctic sea ice loss. J Clim 26:1230–1248

Seo H, Yang J (2013) Dynamical response of the Arctic atmospheric boundary layer process to uncertainties in sea-ice concentration. J Geophys Res Atmos 118:12–383

Serreze MC, Barry RG (2011) Processes and impacts of Arctic amplification: a research synthesis. Global Planet Change 77:85–96

Serreze MC, Barry RG (2014) The Arctic climate system. Cambridge atmospheric and space science series, 2 edn. Cambridge University Press, Cambridge. https://doi.org/10.1017/CBO9781139583817

Serreze MC, Barrett AP, Stroeve JC, Kindig DN, Holland MM (2009) The emergence of surface-based Arctic amplification. Cryosphere 3:11–19

SIMIP (2020) Arctic Sea Ice in CMIP6. Geophys Res Lett 47:e2019GL086749

Simmons AJ, Poli P (2015) Arctic warming in ERA-Interim and other analyses. Q J R Meteorol Soc 141:1147–1162

Stroeve J, Notz D (2018) Changing state of Arctic sea ice across all seasons. Environ Res Lett 13:103001

Stroeve J, Holland MM, Meier W, Scambos T, Serreze M (2007) Arctic sea ice decline: faster than forecast. Geophys Res Lett 34:1–7. https://doi.org/10.1029/2007GL029703

Stroeve J, Kattsov V, Barrett A, Serreze M, Pavlova T, Holland M, Meier WN (2012) Trends in Arctic sea ice extent from CMIP5, CMIP3 and observations. Geophys Res Lett 39:1–7. https://doi.org/10.1029/2012GL052676

Stroeve J, Barrett A, Serreze M, Schweiger A (2014) Using records from submarine, aircraft and satellites to evaluate climate model simulations of Arctic sea ice thickness. Cryosphere 8:1839–1854

Taylor PC, Hegyi BM, Boeke RC, Boisvert LN (2018) On the increasing importance of air-sea exchanges in a thawing Arctic: a review. Atmosphere 9:41

Thackeray CW, Hall A (2019) An emergent constraint on future Arctic sea-ice albedo feedback. Nat Clim Change 9:972–978. https://doi.org/10.1038/s41558-019-0619-1

Vaughan DG et al (2013) Observations: cryosphere. Clim Change 2103:317–382

Vihma T (2014) Effects of Arctic sea ice decline on weather and climate: a review. Surv Geophys 35:1175–1214

Wadhams P (2012) Arctic ice cover, ice thickness and tipping points. Ambio 41:23–33

Webster MA, Rigor IG, Nghiem SV, Kurtz NT, Farrell SL, Perovich DK, Sturm M (2014) Interdecadal changes in snow depth on Arctic sea ice. J Geophys Res Oceans 119:5395–5406

Zhang X, Walsh JE (2006) Toward a seasonally ice-covered Arctic Ocean: scenarios from the IPCC AR4 model simulations. J Clim 19:1730–1747